Controlled generation of vapor-liquid slug flows by local boiling in microgravity

Pau Bitlloch[*]
Universitat de Barcelona, 08028 Barcelona, Spain

Xavier Ruiz[†]
Universitat Rovira i Virgili, 43007 Tarragona, Spain

Laureano Ramírez-Piscina[‡]
Universitat Politècnica de Catalunya, 08028 Barcelona, Spain

Jaume Casademunt[§]
Universitat de Barcelona Institute of Complex Systems, Universitat de Barcelona, 08028 Barcelona, Spain

We design, construct and test a device for controlled boiling by means of local vapor bubble formation in a cavity that injects vapor bubbles in a capillary crossflow. The outcome of the device is a regular slug-flow of approximately monodisperse bubbles that can be used for a variety of applications. The setup is designed to be independent of gravity level and is tested succesfully both in normal gravity and in microgravity using drop tower experiments. The device is calibrated by a systematic study determining the size and frequency of bubble formation as a function of pressure and flow conditions. Results turn to be virtually independent of gravity. Different regimes of operations are identified and described, and basic properties of the behavior of the bubbles inside the nucleation cavity are discussed. The slug flow downstream the crossflow is characterized and shows some differences depending on gravity. Finally we illustrate the use of a controlled regular slug flow generated by our device by using it as an input of a serpentine heat exchanger. This emphasizes an important virtue of our method for practical applications, namely, the ability to separate the process of bubble formation from the actual heat exchange by phase transformation in the region of interest.

---

[*]Post-Doctoral Researcher, Departament d'Estructura i Constituents de la Matèria, Avinguda Diagonal 647.

[†]Professor, Departament de Química, Física i Inorgànica, Marcelí Domingo s/n; josepxavier.ruiz@urv.cat.

[‡]Associate Professor, Departament de Física, EPSEB, Doctor Marañón 44; laure.piscina@upc.edu.

[§]Professor, Departament de Física de la Matèria Condensada, Avinguda Diagonal 647; jaume.casademunt@ub.edu.

Nomenclature

Ca	=	Capillary number
Bo	=	Bond number
Re	=	Reynolds number
g	=	acceleration of gravity
η	=	liquid viscosity
σ	=	surface tension
$\Delta\rho$	=	density difference between vapor and liquid
δT	=	temperature difference
ΔP	=	pressure gap along the bubble
x	=	distance to the pyramid tip
t	=	time since bubble nucleation
v	=	bubble velocity
R, L	=	bubble radius and length
δr	=	wider space left between bubble and wall
$T_{\text{cold Bath}}$	=	cold bath temperature
$T_{\text{med Bath}}$	=	medium bath temperature
$T_{\text{hot Bath}}$	=	hot bath temperature
T_{metall}	=	metallic piece temperature
$P_{\text{effective}}$	=	effective pressure
ϕ	=	co-flow flux

I. Introduction

The study of two-phase fluid flows in microgravity is widely recognized as a strategic area of research for applications in space technology [1], being critical in many aspects of life support systems, power generation and propulsion. Many of such situations involve generic problems in phase mixture/separation, two-phase fluid management and control, wetting and contact line dynamics, phase change, or heat and mass transfer. While these processes are encountered in many engineering fields already in terrestrial conditions, the study in non-terrestrial gravity conditions poses additional challenges from the point of view of fundamental physics, in particular because of the limited access to microgravity platforms and the corresponding lack of high quality data. One of the most critical issues is the development of high performance thermal management systems that take advantage of the large latent heat transportation [2]. In particular, many thermal control systems involve liquid/vapor phase change in flowing conditions, a situation that is known as flow

boiling [3]. Although the interest on flow boiling in microgravity heat transfer is high, the existing experimental data is still quite limited, fragmentary, and often incoherent, while the knowledge of the fundamental physical mechanisms involved is far from satisfactory [4–6]. Research efforts so far have thus been driven by the urgency of the engineering need of quantitative characterization, rather than the fundamental understanding of the physics involved.

The aim of the present work is to focus on situations of flow boiling that are sufficiently simple and controllable so that one can get high quality data, and which can in turn be amenable to scaling analysis and interpretation. In this respect, previous work on the non-thermal case has shown the importance of controlling the generation of the two-phase flow in order to gain insight into the physical mechanisms involved in the resulting flow. In particular the possibility of generating monodisperse bubble suspensions of prescribed size and volume fraction in capillary tubes [7–10] has allowed to have access to a collection of high quality microgravity data about the interaction between bubbles and turbulence in different conditions [11–14]. In this way, a fundamental problem in fluid physics and transport, namely that of turbulent dispersed multiphase flow [15], in the particularly elusive case of non-buoyant dispersed bubbles[16], was brought to the same footing as other more accessible and common two-phase suspensions. In the case of vapor/liquid of the same substance, the combination of turbulent multiphase flow with heat exchange and phase transformation poses a formidable challenge both to theory and experiment. From a fundamental point of view it has been thus imperative to devise analogous methods of creating simple and controlled situations that can serve as basis for effective progress.

Within this spirit here we address the controlled generation of nucleate boiling in a capillary tube by a gravity insensitive procedure, with the practical result of achieving a periodic slug flow of vapor bubbles of nearly monodisperse sizes. Bubbles are nucleated at a specific site and injected into a capillary cross-flow, a situation that we term slug boiling. The geometry and conditions of the nucleation site is designed to achieve two goals: the periodicity of the slug boiling, and the monodisperse size distribution of the vapor bubbles, both in microgravity. This vapor-liquid slug flow is an interesting object of study in itself, but can also be employed as an auxiliary system to supply monodisperse vapor bubbles for subsequent use in different situations and devices, both for fundamental study or practical applications of heat exchange. In particular for heat transfer applications, our slug boiling system offers the interesting possibility of separating the actual formation of the bubbles by nucleation from the heat exchange process by phase transformation. The bubbles are thus formed and transported with a prescribed size and frequency of formation that can be controlled regardless of the gravity level, and can then be subsequently be transported and injected into another device for optimal performance depending on the actual needs, or for fundamental studies under different gravity conditions.

Nucleate boiling induced by microstructured surfaces has been largely studied in normal gravity and usually in static conditions (no externally-induced flow) [17]. On the other hand, in flow boiling, the heat transfer takes place commonly through the walls of pipes or along internal wires. However, localized nucleate boiling under flow conditions in microgravity has not received much attention. In addition slug flows in flow boiling have been rarely observed because of the use of tubes of relatively large diameters, and if so, they were quite irregular [3]. Generation of microbubbles in

microchannels could reach however more regular regimes [18, 19], and the seed of pre-generated bubbles at the 10 μm scale by using active microheaters operating at a controlled frequency has shown the capability of reducing flow instabilities [20].

In this work, we performed a series of drop tower experiments in the ZARM microgravity facility in Bremen, Germany, each consisting of 4.1 seconds of high quality microgravity conditions. The experimental setup was designed to be tested also in normal gravity on ground, to verify the insensitivity of its performance to gravity conditions. Our results show that the combination of nucleate boiling with the use of capillaries reduces dramatically the inherent fluctuations of the nucleation processes and permits the achievement of regular and controlled vapor-liquid slug flows. To do so we designed a pyramidal (wedge-like) nucleating cavity under such conditions that, without any device of active control, it injects a periodic train of vapor bubbles into a capillary flow. We studied in detail, both in microgravity and in normal gravity, the boiling process inside the nucleating cavity and the resulting vapor slug flow in the capillary. As a result we identified three operating modes of the nucleating device depending on parameter regimes, and performed a complete characterization of the resulting slug flow (namely the frequency and the mass flow rate of the generated vapor bubbles) as a function of the injection parameters. The test of our setup in normal gravity showed very similar results to those in microgravity. This should facilitate future experimental research to complete and possibly extend our results without the need of microgravity conditions. To illustrate the practical use of the outcome of our system as a tool for further research, we have completed our analysis with a first characterization of the generated slug flows both in microgravity and normal gravity, showing how the uniformity of the generated bubbles facilitates the detection of small changes suffered by the slug flow along a length of a few centimeters of capillary. Finally, to illustrate the use of previously controlled slug boiling on heat transfer applications, we injected the vapor slug flows generated by our system into a capillary serpentine heat exchanger, in normal gravity conditions. In this case we showed that relevant heat transfer due to phase change is conveniently measured for small temperature differences between the exchanger and the working fluid, without the need of involving uncontrolled bubble nucleation inside the exchanger.

The outline of this papers is as follows. In Section II we describe the nucleating device and the experimental set-up, in Section III we show the obtained results, and in Section IV we summarize the conclusions.

II. Description of the experimental setup

The main objective of the experiment is to achieve the generation of controlled slug-flows of vapor-liquid bubbles in a capillary tube and its proper performance in microgravity. To do so a nucleating cavity is constructed in a pyramidal shape, of length of the order of a few millimeters, and width of the order of a fraction of millimeter. The portion nearest the tip of one of its faces is a heated metallic surface, and the rest of surfaces are heat insulating except the base of the pyramid which opens to a capillary crossflow of preheated liquid. The nucleation of the vapor bubbles occurs at the narrow part of the cavity, in contact to the hot metallic surface. Due to the small size the dynamics of the bubble
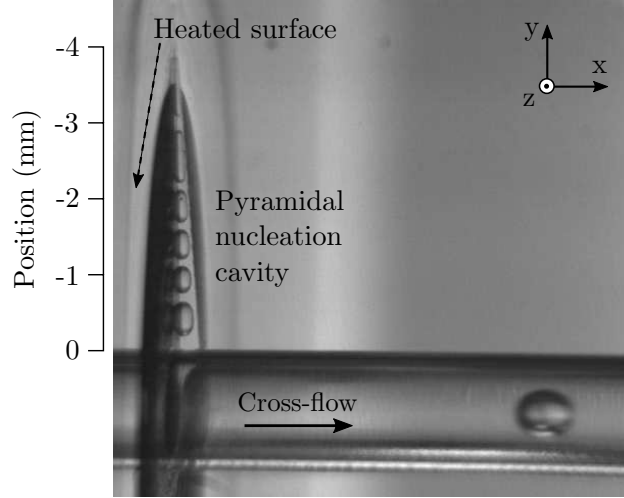
Fig. 1 **Snapshot seen from above of the nucleating device in microgravity conditions. At left it can be seen the pyramidal cavity, with the train of vapor bubbles moving towards the horizontal capillary at the bottom. Cavity is limited at left by a vertical plane, corresponding to the surface shown in Fig. 4, in which it can be distinguished the insulating part, as a darker area, from the (reflecting) metallic part labeled as "Heated surface". Vertical direction of experiment corresponds to the z direction (perpendicular to the image). The scale indicates position of bubbles respect to the exit point as used in Subsec. III.A. This particular cavity corresponds to the Wide Isolator case of Subsec. III.A.**

inside the cavity is dominated by capillary forces. Therefore the growing of the bubbles, due to phase change, drives the

bubble to the wider part of the pyramid and hence induces its injection into the capillary crossflow. An actual snapshot

of the nucleation cavity performing in microgravity can be seen in Fig.1.
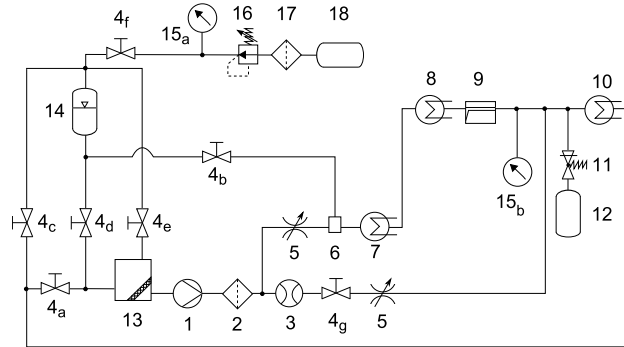

Fig. 2 **Schematics of the experimental setup. 1-Liquid pump, 2-Liquid filter, 3-Liquid flow-meter, 4-Manual valve, 5-Manual throttle, 6-small receptacle of liquid, 7-Medium bath, 8-Hot bath, 9-Measuring area, 10-Cold bath, 11-Pressure limited valve, 12-security reservoir, 13-Phase separator, 14-Liquid reservoir with air pressure, 15-Manometer, 16-Pressure regulator valve, 17-Air filter, 18-Pressured air reservoir. Standard experimental configuration requires the manual valves 4a, 4b, 4f and 4g open, while the rest are closed. Other configurations exist exclusively for the preparation of the experiment. Level of liquid in (14) is fixed to be the same height of the nucleation cavity, in order to prevent changes of hydrostatic pressure at that location in microgravity. Cold bath (10) must also be at the same level, otherwise the lost of hydrostatic pressure would interact with the vapor accumulated in this region, affecting the flow rate of the whole experiment**

Schematics of the experiment can be found in Fig.2. The liquid used (fluorinert FC-72) is pre-warmed in its flow

through two hot baths in order to increase its temperature in a controlled manner. The first one (stainless steel, 3 mm inner diameter, 6 loops, roughly 2.1 m of pipe length inside the bath, labeled as "Medium bath" in the figure) heats up the flow up to a value close to the boiling point, then the second one (stainless steel, 1.5 mm inner diameter, 8 loops, roughly 2.8 m of pipe length inside the bath, labeled as "Hot bath" in the figure) carefully rises that temperature up to the boiling point or even overheat the liquid a little above that point. That second bath needs to be carefully prepared in order to prevent scratches or any other kind of potential nucleation points that could lead to a chaotic generation of bubbles in undesired places.
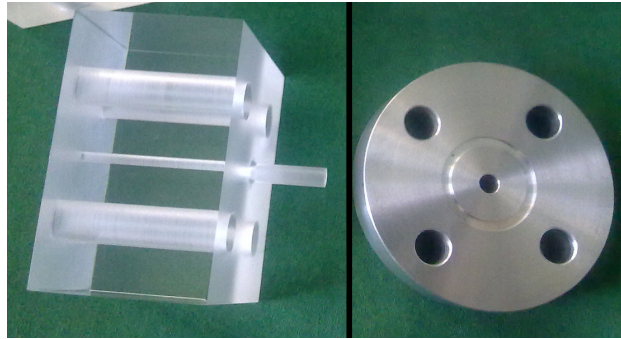

Fig. 3   Left: plexiglass piece constituting the end of the capillary tube coming from the second bath; Right: heating metallic piece to be inserted around the final part of the first plexiglass tube. Note that by using this setup the liquid in the capillary does not enter directly in contact with the heater.
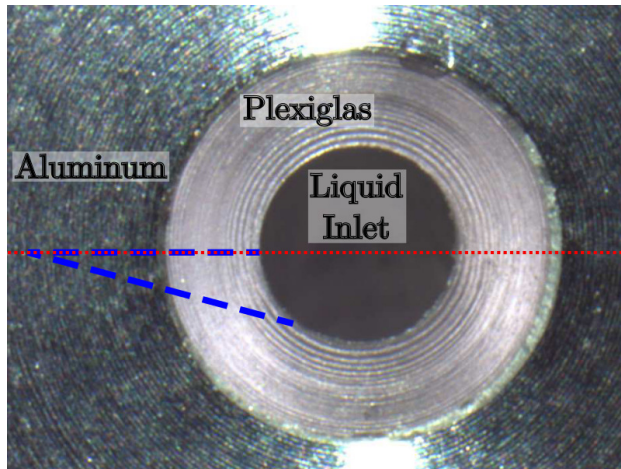
Fig. 4   Close-up of the heated wall of the pyramidal cavity, formed by the two pieces of Fig. 3 mounted together. Blue dashed lines indicate one example of nucleation cavity once the two pieces of the second capillary (see Fig. 5) were assembled. Red dashed line indicates the position of the union of the two pieces of the second capillary.

The tube exiting from the bath is connected to a transparent capillary tube of 1.5 mm inner diameter by using an intermediate device. The pyramidal nucleation cavity is constructed in the union of this device and the second transparent tube. This intermediate device is formed by two pieces of different materials (plexiglass and aluminum, see Fig. 3) and its geometry is as follows. The first tube finishes in the plexiglass piece (Fig. 3 left), in which it can be
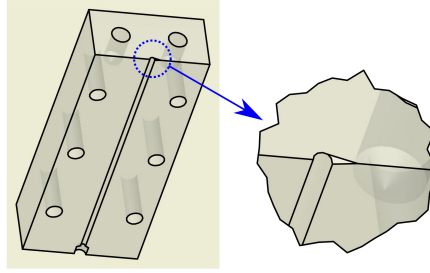
Fig. 5 **Schematics of one of the parts of the second (transparent) capillary with a semicircular drill for the capillary pipe tube. In one extreme a small cut for the nucleation cavity is performed. The other part of the second capillary is identical, except that it has not such small cut.**

observed a prolongation of the capillary. Around this prolongation it is mounted the cylindrical aluminum piece (Fig. 3 right) with a central hole in which the prolongation of the plexiglass piece is inserted. This aluminum piece will be heated for the nucleation process. The ensemble of both pieces, once inserted, present a common planar surface (at the end of the plexiglass prolongation) in whose center it is found the tube orifice, as can be seen in Fig. 4. This is directly attached to the referred second transparent capillary tube. It is the slug flow in this second capillary which is either observed and measured, or injected into an additional device. This transparent capillary is constructed with a set of two pieces of plexiglass, each of which has impressed a semi-cylindrical drill (1.5 mm diameter) that will constitute the capillary tube when both parts are mounted together (Fig.5). In one of the parts, a small planar cut (typically with a length of 4.75 mm from the center of the capillary, and in its wider end with depth 0.32 mm and width 0.75 mm) is performed to create the pyramidal cavity. Thus, the cavity will be formed by both plexiglass parts and a third side partially made out of aluminum that will be heated to force the boiling in there.

In Fig. 4 it can be seen the surface of the end of the first capillary, formed by the aluminum and the plexiglass pieces. Here the blue dashed lines show the shape of one of the sides of the pyramid, being the base of it open to the liquid inlet coming from the hot bath. Notice in that figure that the closest region to the capillary tube of the visible face of the pyramid is made out of plexiglass. That is done to prevent unwanted nucleation of bubbles directly inside the tube. Being plexiglass a bad thermal conductor it restricts the nucleation to happen exclusively on the metallic region of the cavity. The design of this insulating piece was a crucial point in the development of the experiment, being the only way found to prevent spurious nucleation happening outside the nucleation cavity. Moreover for the experiments we have used different pairs of aluminum/plexiglass pieces with different thicknesses of the insulating part (but the same inner diameter) in order to have results for pyramidal cavities with different metallic/insulating lengths. Specifically three external diameters for the insulating part were used: 3 mm, 5 mm and 8 mm, with an internal diameter of 1.5 mm corresponding to the capillary width.

In order to minimize the differences in the performance of the system when changing the degree of gravity, one of

the sides of the pyramid is placed as a ceiling of the nucleation cavity, transverse to gravity. This is achieved by placing horizontally the union plane between both pieces of the second capillary (red line in Fig. 4), and performing the small cut on only the piece below. In that way when bubbles are generated in normal gravity conditions they only feel a higher force towards that horizontal wall, instead of taking advantage of buoyancy forces to help them detach or move. Under these conditions the deformation of the bubble due to gravity is controlled by the Bond number Bo = $\Delta\rho\, g\, L^2/\sigma$. In this setup, taking L as the maximum transversal dimension at the cavity outlet, Bo $\simeq$ 1. Note that for the most part of the cavity the effective Bond number is much smaller.

The exit of the tube where the slug-flow is observed is connected to the return of the flow of the bypass. Since that is cold liquid it helps to condensate the vapor and to increase the flow rate through the cold bath, preventing the unwanted accumulation of vapor in any region.

III. Bubble nucleation and dynamics in the pyramidal cavity

A. Single-bubble dynamics
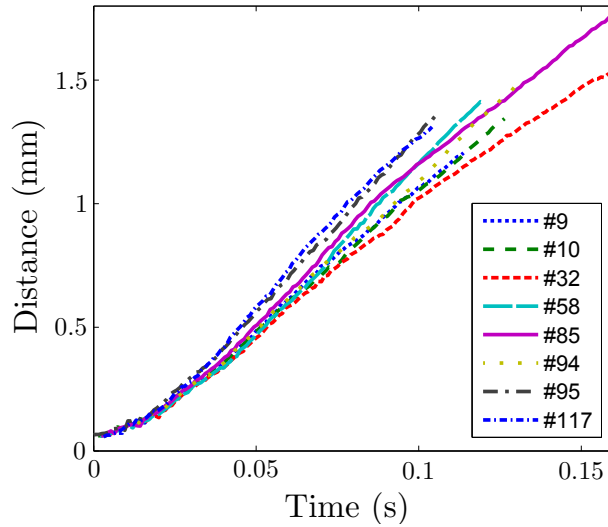
Fig. 6   Characteristic trajectories of bubbles in contact with the metallic surface inside the nucleation cavity, as a function of the time since they have been created, in microgravity experiments. Trajectories of each bubble end when the bubble suffers a coalescence.

For the discussion and interpretation of the experimental results it is useful to analyze first the limiting case where a prediction can be made. This is the case of a single bubble growing and displacing in a wedged-shaped cavity with perfectly conducting walls, in the limit dominated by surface tension over viscous forces (small capillary number Ca = $\eta v/\sigma$) and negligible inertia (small Reynolds number Re = $\rho v L/\eta$). Under these conditions, we may assume that there is a constant temperature difference δT between the vapor and the liquid, and therefore that the volume growth rate of the bubble, proportional to the heat flux over its surface, is in turn proportional to the bubble surface area. The fact

that Ca≪ 1 will ensure that the bubble shape remains invariant and, as we will see shortly, it moves at constant speed along the opening direction of the wedge.

In fact, for any opening geometry of the cavity such that the transversal section preserves its shape and its lateral dimension increases linearly with distance to the tip (be it a pyramid, a cone, or a wedge) the shape of the bubble will be asymmetrical, and thus generate a capillary pressure drop different in the front and the rear. The pressure difference on both sides will be balanced by the viscous flow around the bubble towards the rear and thus driving the bubble toward the opening direction. We may assume that the size of the bubble will adapt to the lateral size of the opening tube at its specific location, while keeping the shape, hence it will be proportional to the distance x to the tip. Accordingly, the volumetric growth rate (proportional to the surface area) will be proportional to $x^2 \delta T$. Similarly, since the volume is proportional to x^3, the volumetric growth rate will be proportional to $x^2 v$, being $v = dx/dt$ the bubble velocity. Thus in these conditions v should be constant and proportional to δT.

It remains to be justified that the invariance of the bubble shape is consistent with a constant bubble velocity. To this end, note that at such small scales the movement of a bubble should be the result of a balance between capillary and viscous forces. Capillary forces depend on the bubble shape, so the resulting shape is the result of such balance. We will see now that for an invariant shape this balance is not broken during the growth and movement of the bubble if its velocity is constant. On the one hand capillary pressures boosting the bubble are proportional to $1/R \sim 1/x$. On the other hand the pressure gap necessary to drive the liquid with viscosity η from one end to the other of the bubble (permitting it to advance) is $\Delta P \sim \eta v L / \delta r^2$, being δr a scale of the order of the wider space left between the bubble and the wall and L the length of the bubble, both proportional to x if the bubble shape is invariant. This results in $\Delta P \sim \eta v / x$. Since $\Delta P \sim 1/R \sim 1/x$, the balance between capillary and viscous forces can be maintained for a shape-invariant bubble if v is constant. That means that the bubble volume is proportional to the cube of its life time ($V \propto t^3$) or, equivalently, to the cube of its distance to the cavity tip.

This analysis can be extended in principle to a train of bubbles, but if they are too close, coalescence events may take place. In the event of a coalescence of two bubbles, a larger bubble is formed and will deform and move rapidly to the location corresponding to the new current volume and then adopt the velocity corresponding to the new location. It may happen that in the fast displacement following the coalescence, new bubbles are encountered and new coalescences may be generated. In the experiments bubbles are nucleated in the hot metallic part of the pyramidal cavity, and grow according to the physical picture of a self-similar train of bubbles described in this Sec. III.A, with occasional coalescences. Depending on the experimental parameters, other different regimes of growth can be found as it will be analyzed in detail in Sec. III.B.

We have performed experiments using different thicknesses of the capillary of the plexiglass insulator piece shown in Fig. 4 in order to characterize and differentiate the bubble dynamics in both parts (*i.e.* metallic and insulating parts) of the cavity. For the case of the smallest thickness of the insulating part we show in Fig. 6 the trajectories of some

9

characteristic bubbles inside the nucleation cavity. It can be seen how, in contact with the metallic hot surface, after an initial short transient they reach a roughly constant velocity.

When larger thicknesses of the plexiglass part are used, the movement of the bubbles in contact with the metallic part is observed to follow the trends described above, but when bubbles are in contact with the insulating part their dynamics is quite different. First of all, the bubble volume no longer increases as x^3 but, depending on the case, a weaker increase or even a decrease can be observed. Note that the reduced bubble volume in the insulating part, compared to the invariant shape of the metallic case, should have an impact on its velocity. Since the bubble is in this case smaller in relation to its position in the cavity, its degree of deformation is smaller, and so will be the capillary forces and hence its velocity. This effect could be expected, by noting that along the insulating part of the cavity, a temperature gradient will be present between the hot metallic part and the colder transverse crossflow. Therefore the temperature gap with the vapor phase of the bubble is expected to decrease towards the exit of the cavity, and hence also the bubble velocity. As a consequence the shape invariance discussed above will be lost, and the bubble size will no longer be expected to scale with the cavity width.
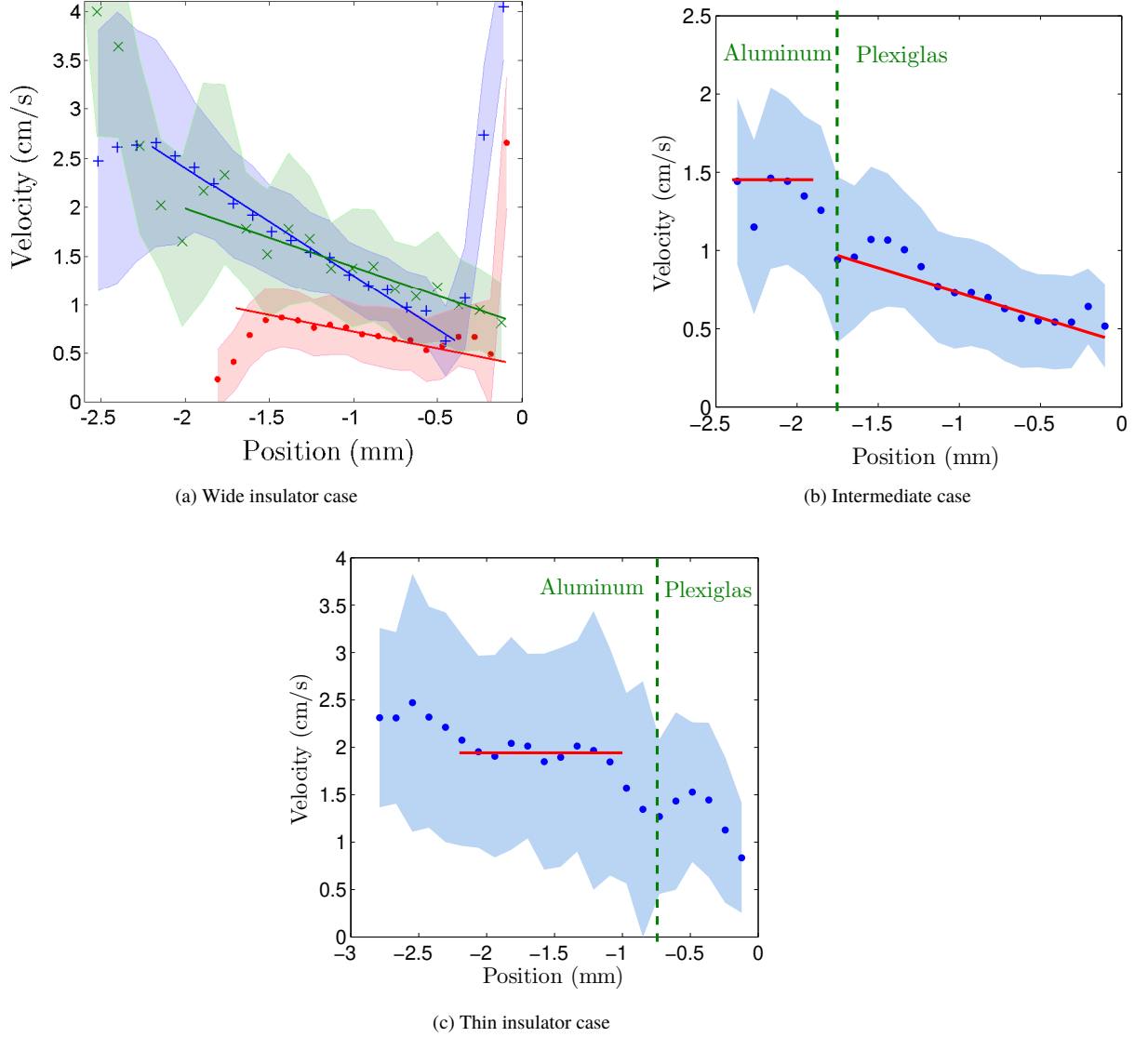
In Fig. 7a some results for a case with smallest metallic part are shown. Here we observe a linear growth of bubble volume with distance along the larger insulating part. When using smaller thickness of insulator it can be observed in Fig. 7b how the volume growth of bubbles is cubic in the metallic part, while it is linear, after a transient, in the insulating part. Reducing further the insulating part (Fig. 7c) we see that after the cubic growth on the metallic part a roughly linear decreasing of volume on the insulating part is observed.

Accordingly Fig. 8a shows for the case of the largest insulator width a clear linear decay of velocity with distance. Figs. 8b and 8c show also the transition between metallic and insulating parts. While in the insulating part a linear decay is also observed, in the metallic part a zone with roughly constant bubble velocity can be identified. In these cases we observe a tendency for a number of bubbles to nucleate at the contact point between metallic and plexiglass parts, so mean values near that point are affected by bubbles that were nucleated there and remain at rest until their growth starts to drive them towards the wide part of the cavity.

We also remark that in Figs. 7 and 8 the dispersion of volumes and velocities are relatively small in all cases. Note that the relative dispersion in the lateral dimension of the generated bubbles is one third of that of the volume. Consequently the distribution of bubble sizes generated by this procedure is effectively monodisperse to a good approximation. To better illustrate this point we show in Fig. 9 typical results for the distribution of equivalent radius (calculated from the measured volumes assuming a spherical shape). We show two representative cases, in Fig. 9a a wide insulator case (corresponding to the case in Fig. 7a-red), and in Fig. 9b a thinner insulator case (corresponding to Fig. 7b). The dynamics inside the cavity is such that capillary forces tend to locate a bubble of a given size at a corresponding position such that it always fills the same fraction of the cavity section. Due to this mechanism, the dynamics is effectively reducing the dispersion originated by the nucleation process, and producing a fairly monodisperse distribution of sizes.

10

(a) Wide insulator case

(b) Intermediate case

(c) Thin insulator case
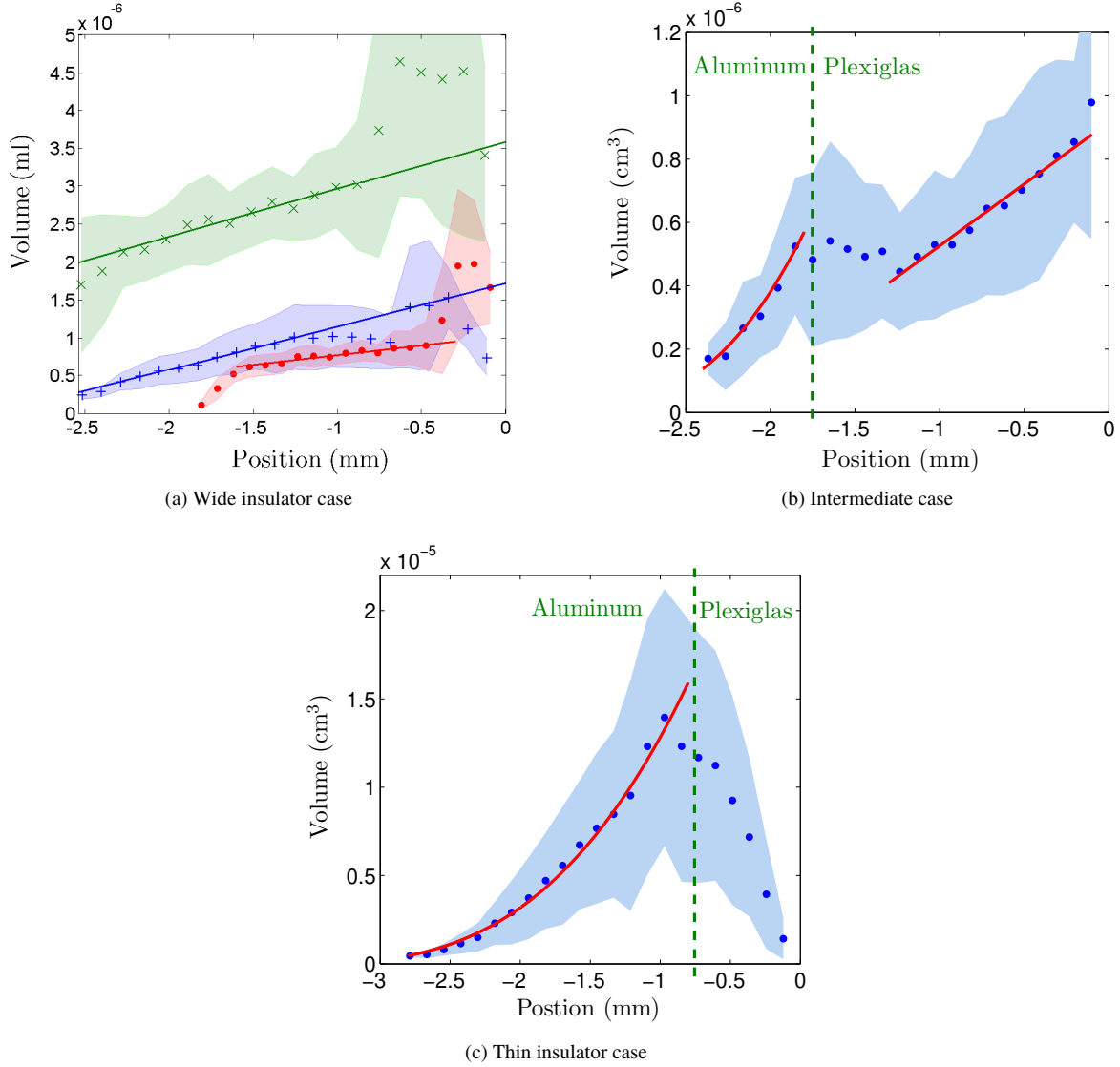
Fig. 7   Mean bubble volume as a function of the position in the nucleation cavity, for several widths of the insulator tube, in microgravity experiments.   (a) widest insulator tube; (b) intermediate case;(c) thinnest insulator case. Position 0 corresponds to the entrance to the transverse capillary tube. Vertical lines indicate the transition from plexiglass to metallic heated surface in each case (in (a) only the insulating part is shown). For the case (a) the three sets of results shown correspond to different drops with different flow, temperature and pressure conditions. For the case (b) a deeper (0.48 mm depth) pyramidal cavity was used. Solid lines in isolated parts are linear regressions of significant points. Solid lines in metallic parts are cubic fits. Colored areas correspond to the standard deviation of the results. The scales for standard deviation are the same as for each magnitude. (a) red: $T_{\text{cold Bath}} = 37.4^o\text{C}$, $T_{\text{med Bath}} = 57.9^o\text{C}$, $T_{\text{hot Bath}} = 59.8^o\text{C}$, $T_{\text{metall}} = 57.8^o\text{C}$, $P_{\text{effective}} = 1.000$ **bar,** $\phi = 53$ **ml/min; blue:** $T_{\text{cold Bath}} = 32.5^o\text{C}$, $T_{\text{med Bath}} = 58.6^o\text{C}$, $T_{\text{hot Bath}} = 60.0^o\text{C}$, $T_{\text{metall}} = 60.7^o\text{C}$, $P_{\text{effective}} = 1.042$ **bar,** $\phi = 21$ **ml/min; green:** $T_{\text{cold Bath}} = 30.9^o\text{C}$, $T_{\text{med Bath}} = 58.7^o\text{C}$, $T_{\text{hot Bath}} = 60.2^o\text{C}$, $T_{\text{metall}} = 59.9^o\text{C}$, $P_{\text{effective}} = 1.015$ **bar,** $\phi = 29$ **ml/min; (b)** $T_{\text{cold Bath}} = 36.2^o\text{C}$, $T_{\text{med Bath}} = 58.1^o\text{C}$, $T_{\text{hot Bath}} = 59.8^o\text{C}$, $T_{\text{metall}} = 62.3^o\text{C}$, $P_{\text{effective}} = 1.050$ **bar,** $\phi = 40$ **ml/min; (c)** $T_{\text{cold Bath}} = 30.1^o\text{C}$, $T_{\text{med Bath}} = 58.7^o\text{C}$, $T_{\text{hot Bath}} = 60.2^o\text{C}$, $T_{\text{metall}} = 61.5^o\text{C}$, $P_{\text{effective}} = 1.015$ **bar,** $\phi = 29$ **ml/min.**

11

(a) Wide insulator case


(b) Intermediate case

(c) Thin insulator case

Fig. 8   Mean bubble velocity as a function of the position in the nucleation cavity in microgravity experiments for the same cases as in Fig. 7. Position 0 corresponds to the entrance to the transverse capillary tube. Vertical lines indicate the transition from plexiglass to metallic heated surface in each case. Solid lines in (a) are linear regressions of significant points. In the rest of cases solid lines are guides to the eye. Colored areas correspond to the standard deviation of the results. The scales for standard deviation are the same as for each magnitude.

(a) Wide insulator case

(b) Intermediate case
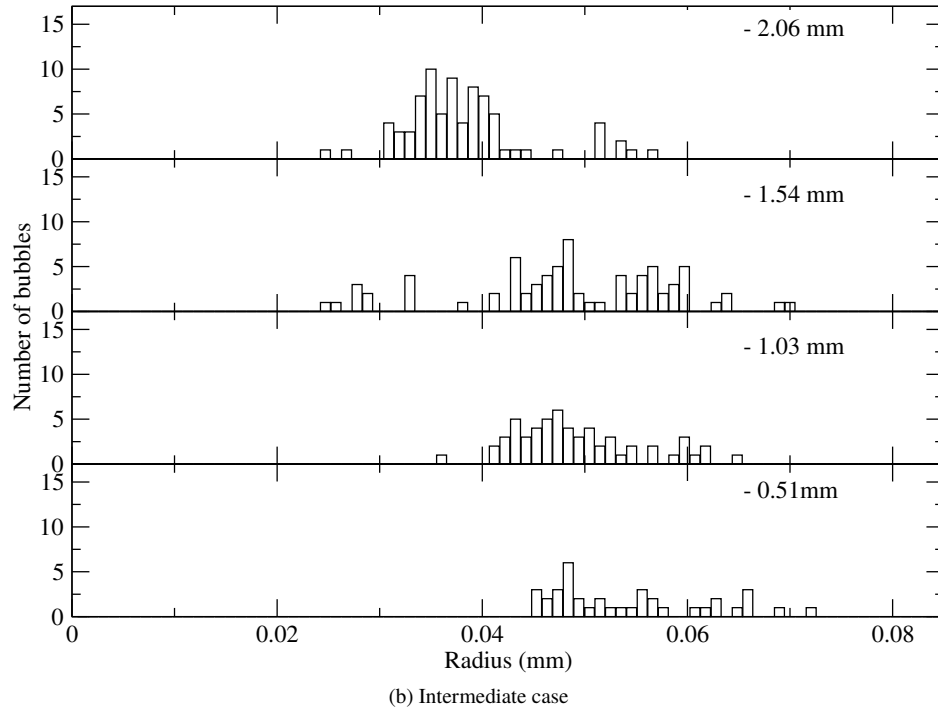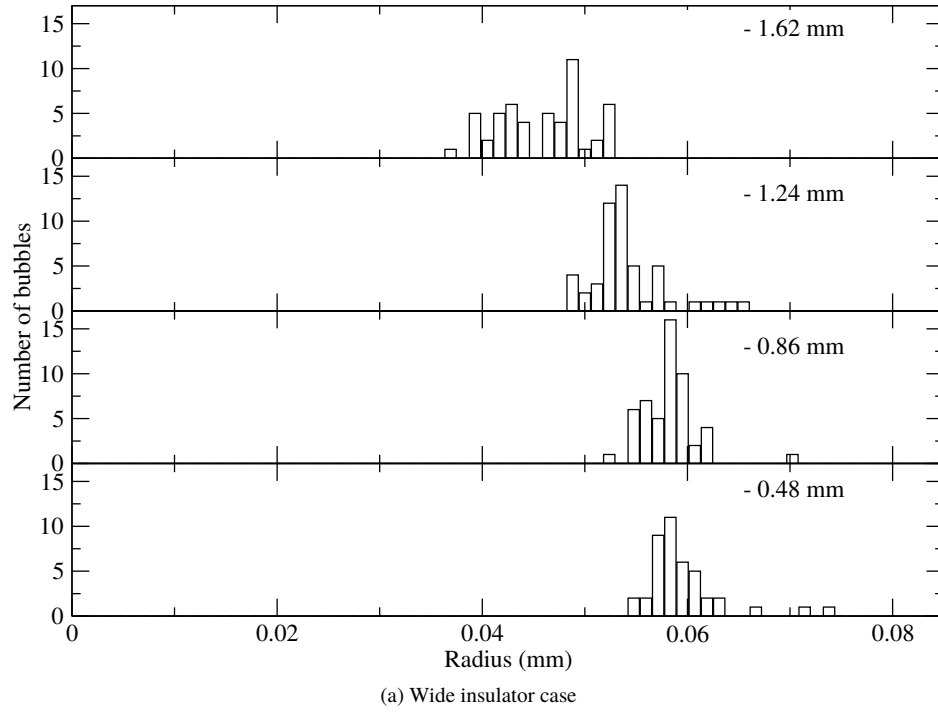
Fig. 9 Distribution of equivalent radius calculated from the measured volumes assuming a spherical shape, corresponding to bubbles crossing different points along the nucleation cavity. Distances from the cavity exit are indicated for each position. (a) case corresponding to Fig. 7a (red); (b) case corresponding to Fig. 7b.

In the thinner insulator case (Fig. 9b) the nucleation is more erratic, which produces a noisy distribution, but the dynamics is able to improve the distribution near the exit of the cavity. Our results for size distributions are noisy due to relatively poor statistics, and are included for illustrative purposes. A more systematic study is beyond the scope of this work.

B. Nucleation characterization of the cavity
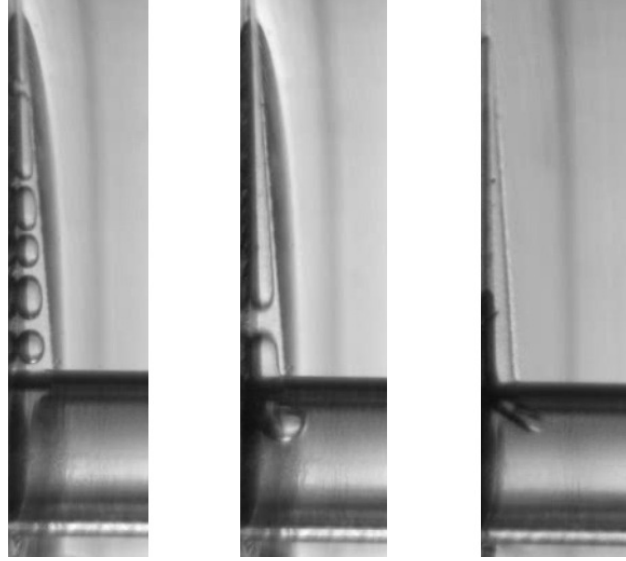
Fig. 10   Three modes of nucleation in the tethraedral cavity, obtained from experiments performed in micro-gravity: (Left) Mode A: train of small bubbles; (Center) Mode B: single large bubble detaching smaller ones which are pushed to the crossflow; (Right) Mode C: cavity full of vapor, detaching bubbles to the crossflow due to drag forces

A series of experiments have been performed by varying the liquid flow rate of the crossflow and the pressure of the system, but maintaining constant the temperature parameters: $T_{\text{cold Bath}} = (33 \pm 3)°C$, $T_{\text{med Bath}} = (58.5 \pm 0.5)°C$, $T_{\text{hot Bath}} = (60.0 \pm 0.5)°C$, $T_{\text{nucleation wall}} = (66.5 \pm 0.5)°C$. The actual pressure P at the nucleation cavity is determined from measurements elsewhere taking into account hydrodynamic corrections due to Venturi effect and viscous pressure along the pipes of the setup, and also thermal corrections. In order to compensate for slight variations of temperature for different experiments, due to the difficulty to impose a fixed temperature of the metallic surface, we define an effective pressure $P_{\text{effective}}$ that incorporates the variation of vapor pressure according to the Clausius-Clapeyron equation. In this way results obtained at slightly different temperatures can be properly compared.

Three main operating modes of the pyramidal cavity have been identified, as shown in Fig. 10. The boundaries in parameter space between these bubble generation regimes are indicated in Figs. 11, 12. The first one (Mode A, left picture in Fig 10, top region in Figs. 11, 12) is characterized by the nucleation of small bubbles which grow and move through the cavity as discussed in the previous subsection. This mode occurs for the largest effective pressures and is
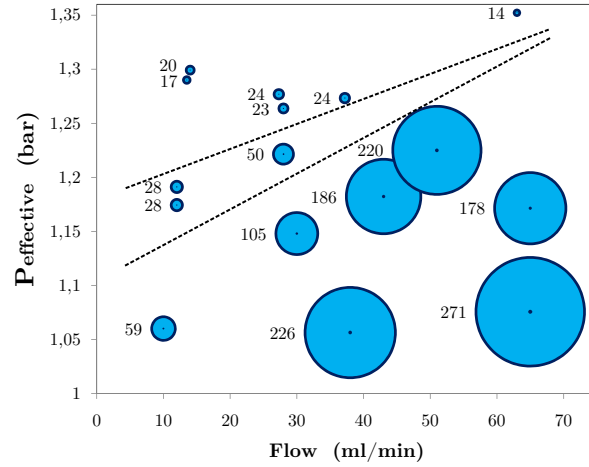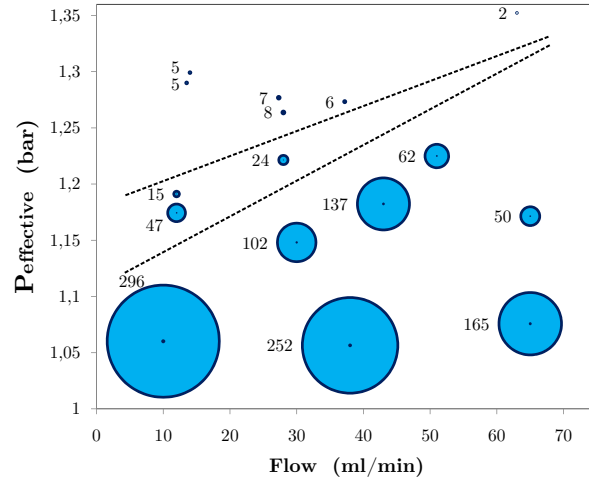
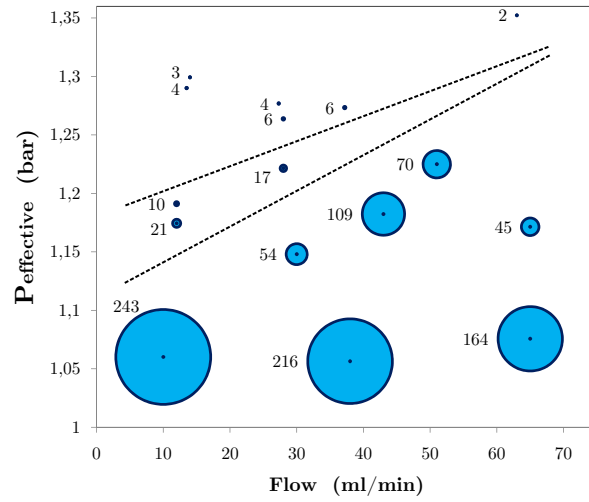(a) normal gravity conditions
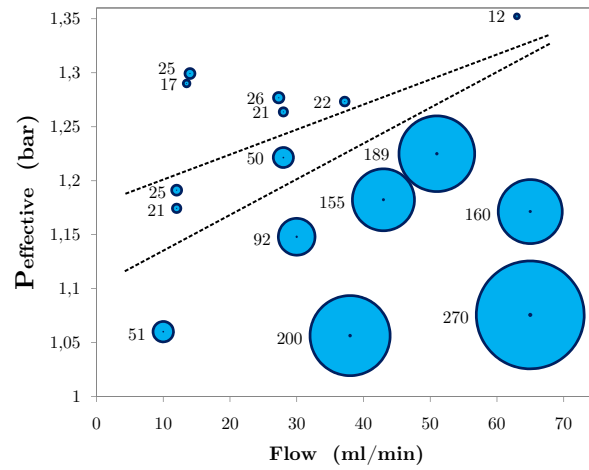
(b) microgravity conditions

Fig. 11 Diameter of circles indicates the frequency of bubbles getting out of the nucleation cavity for a given flow rate and pressure (corresponding values of number of bubbles per second shown next to each circle). Experiments performed in normal gravity conditions (a) and microgravity (b) are compared. Dashed lines separate the three modes of bubble generation: from top to bottom Modes A, B and C (see text)

favored by small values of crossflow. On the opposite extreme case (Mode C, right picture in Fig 10, bottom region in Figs. 11, 12), the cavity is always completely filled with vapor. In that case drag forces originated by the crossflow at the junction cause the detachment of bubbles into the transverse capillary, forming a slug-flow of small bubbles. Then the resulting bubble formation is the result of the balance between capillary and drag forces, in a way very similar to the non-thermal case described in Ref. [7]. This case is observed for the smallest effective pressures and is aided by large crossflows. The third case is in between the previous two (Mode B, center picture in Fig 10, middle region in Figs. 11, 12), corresponding to intermediate values of the effective pressure and not very large flows. In this case the cavity is almost completely full of vapor but is detaching smaller bubbles near its wider end. These small bubbles are

(a) normal gravity conditions

(b) microgravity conditions

Fig. 12 Diameter of circles indicates the mass flow rate of vapor getting out of the nucleation cavity for a given flow rate and pressure (corresponding values in μg/s shown next to each circle). Experiments performed in normal gravity conditions (a) and microgravity (b) are compared. Dashed lines separate the three modes of bubble generation: from top to bottom Modes A, B and C (see text)

periodically injected into the crossflow.

In Fig. 11 we show a comparison of the effect of gravity in the frequency of bubbles leaving the nucleation cavity. It can be seen that gravity seems to have a negligible impact onto the bubble generation frequency. In addition to that, in the Mode C (lower region in Figs. 11, 12) there is a clear tendency on increasing the frequency of generated bubbles when increasing the injected liquid flow rate. Changes in pressure seem to have a lesser impact provided that the system remains operating in the same mode of bubble generation.

In Fig. 12 an equivalent comparison is presented for the mass flow rate of generated vapor. This has been estimated

from the measured volume of the generated bubbles once injected into the capillary, by assuming them to be at boiling point temperature and to behave as an ideal gas, and using the Clausius-Clapeyron equation. From the results it is clear that a reduction in the applied pressure gives as a result an increase in the amount of mass changing phase. When the results of Mode C in this figure are compared with results shown in Fig. 11 we see that, at higher flow rates, we obtain a higher frequency of smaller bubbles than at slow flow rates, but that the total mass of liquid evaporated is roughly the same. Figs 11 and 12 are a complete calibration of the performance of the nucleation cavity and constitute the central result of our study.

C. Characterization of the slug flow in the capillary
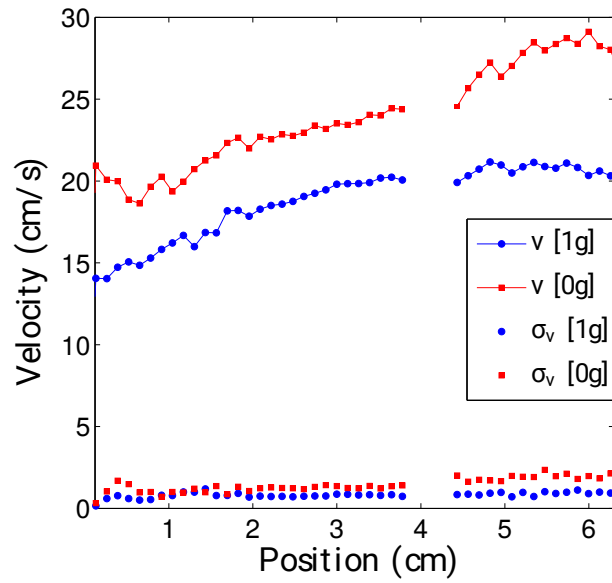
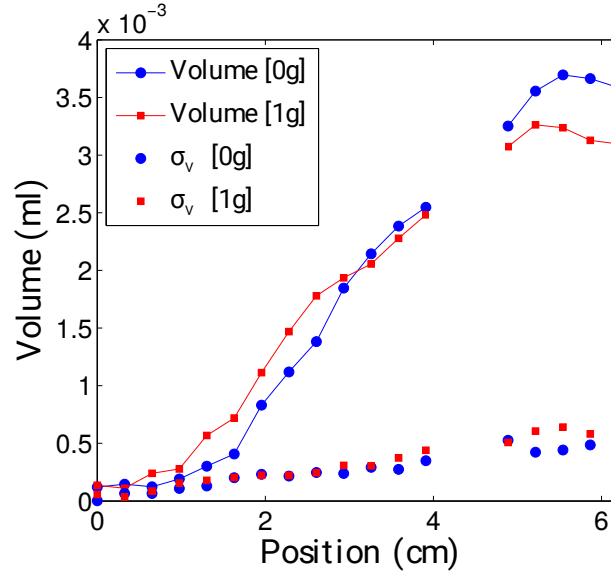

Fig. 13   Mean value and standard deviation of bubble velocities in the generated slug flow in the capillary, as a function of its distance to the nucleating cavity. Blue points: ground experiments; red points: microgravity experiments. Some points around 4.25 cm are missing due to an optical obstacle between the camera and the capillary

Once injected into the capillary, vapor bubbles form a slug flow and are transported by the liquid. During the flow both size and shape of the bubbles can change. This kind of changes of the slug flow characteristics downstream are mainly associated to phase change, depending on the particular thermal conditions along the pipe, and hence their study and control is most relevant regarding practical applications. The monodispersity of bubble sizes and regularity of bubble-bubble distance should facilitate the measurements of small changes, and are thus desired features for this kind of study. In our experiments, for illustrative purposes we have particularized a single case and performed some measurements on the characteristics of the slug flow along a horizontal pipe. To do so we have taken images of the transparent capillary after the cavity and measured positions and shapes of bubbles in different positions along it, and have compared the microgravity and the normal gravity cases.

17
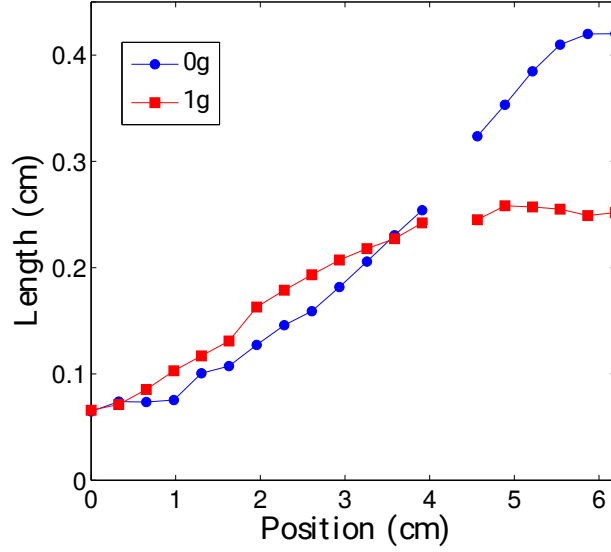
Fig. 14 Bubble length mean in the slug flow as a function of the distance to the nucleating cavity. Red points: ground experiments; Blue points: microgravity experiments.


Fig. 15 Mean value and standard deviation of bubble volumes in the slug flow, as a function of its distance to the nucleating cavity. Red points: ground experiments; blue points: microgravity experiments.

The first obvious effect of microgravity on the slug flow is that, due to the loss of buoyancy forces, bubbles travel through the center of the pipe, as opposed to their behavior in normal gravity, where bubbles travel pressed against the pipe top, thus moving at a smaller velocity as seen in Fig. 13. The velocity of bubbles is clearly increasing along the pipe, which could be associated to a transient for reaching a steady velocity but also to a continuous change in bubble size (see Sec. III.D). Note the low value of the dispersion of measured velocities.

In addition to the change in speed, we observe that, in microgravity, bubbles traveling at the center of the pipe are

18

more elongated than in the case of normal gravity. This is shown in Fig. 14, where it can be seen that, on ground, the elongation of bubbles stops around the position 4 cm, whereas in microgravity conditions this continues during nearly all the observed length. However, even though bubbles elongate more in microgravity, by performing an estimation of the volume of these bubbles we conclude that volumetric growth is not significantly enhanced in microgravity (Fig. 15). Note again in Fig. 15 that the dispersion of results is very small, permitting a fairly clean study of small trends and changes, thanks to the monodispersity of sizes of the generated bubbles.
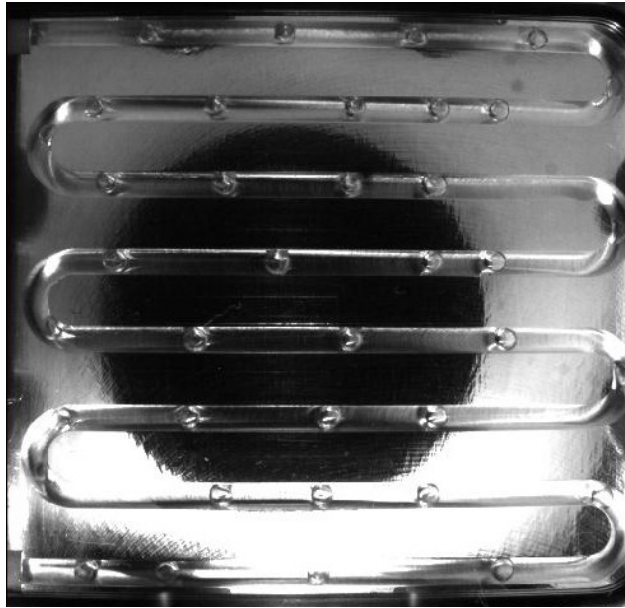

Fig. 16   Heat exchanger. It can be seen the slug flow with small vapor bubbles in the serpentine. Image taken in normal gravity.

D. Heat exchanger

In order to illustrate the use of a pre-generated vapor slug flow for practical thermal transfer applications, we have added a simple heat exchanger connected to the end of the pipe where the slug-flow has been observed (10 cm downstream from the nucleation cavity). The heat exchanger is a serpentine consisting of 8 stretches of 3 cm each with a squared section of side 1.5 mm, drilled in aluminum and covered with a planar plexiglass surface. A picture of the device is shown in Fig. 16. The aluminum surface was heated at different temperatures using a heater cartridge. No significant differences are expected for the behavior of the heat exchanger with changes in gravity level, so due to the limited available access to the microgravity platform we present here results obtained on ground only.

Calibration of the device, to compensate the measurements for heat power losses, was performed by first measuring the power needed for maintaining a constant temperature with a stationary flow. This was done with liquid at high pressure in order to suppress phase change, and repeated for several temperature values. For each fixed liquid flow the power required was linear in the temperature difference $\Delta T = T_{\text{metal}} - T_{\text{liquid}}$. A linear regression of the results permitted
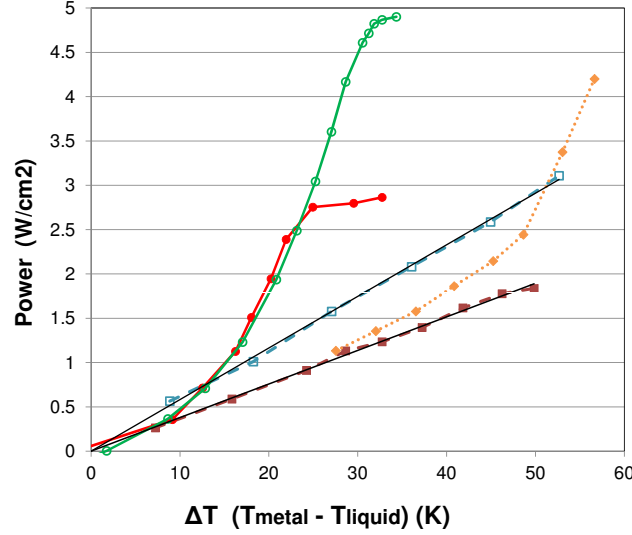
Fig. 17 **Heat power transferred to the fluid in the exchanger as a function of the temperature difference between entering fluid and metal, in normal gravity experiments. Results are corrected by subtracting energy loses. Squares: cold liquid without phase changes; crossflows of 0.5 ml/s (brown), 1 ml/s (cyan); linear fits indicated by black straight lines. Orange diamonds: cold liquid but with phase change nucleated in the serpentine, crossflow of 0.5 ml/s. Circles: preheated liquid with slug flow of small vapor bubbles generated in the piramidal cavity; crossflows of 0.333 ml/s (red), 0.667 ml/s (green). For cold entering liquid the temperature was roughly the same in all cases (27-29.6°C). For hot liquid cases the temperature was close to the boiling temperature (56°C). In the cases without bubbles a large increase of pressure was applied, enough to inhibit boiling.**

to find the power lost to the environment for each corresponding metal temperature. These measured losses were used to correct the results of all the experiments and obtain the values of the heat transferred to the fluid.

As seen in Fig. 17, the experiments performed without phase change indicate that the total heat exchanged was larger for larger flows. This is consistent with the fact that, for larger flows, the liquid suffers a lesser increase of temperature during its shorter transit time through the exchanger, and therefore the temperature difference with the metal is higher, permitting a larger heat transfer.

By injecting a pre-generated slug flow of liquid-vapor at the boiling temperature, the initial slope of the power vs ΔT, plotted in Fig. 17, seems to be similar to the case without phase change. However, with very low ΔT, an increase of heat transfer power is observed. Difference of the corresponding curves for the same flow are attributed to the phase change, which could be observed associated to the growth of the injected vapor bubbles. Thus the slug flow was able to enhance the transfer of heat by phase change without the need of new vapor nucleation inside the exchanger, with small temperature differences. On the contrary, when only liquid is injected, a much larger temperature difference is needed in order to observe phase change significantly contributing to heat transfer. Note that by separating the bubble nucleation problem from the actual heat transfer, one is free to tune the former in order to optimize the latter, thus opening new possibilities for improved performance.

It is noteworthy that this increase in heat transfer due to phase change does not appear to depend on the injected flow,

20

until a saturation (whose value does depend on the flow) is reached. The explanation lies in the fact that when the vapor is already nucleated, all the transferred heat is invested in phase change (there is no need to further vapor nucleation). Then the liquid temperature is constant (the boiling temperature) along all the serpentine, and so is the temperature difference between the liquid and the metal. Therefore the heat transfer is also constant and independent of the flow value, as long as there is still liquid present along all the pipe. However, if the heat transferred is sufficient to vaporize all the liquid, then there will be a portion of the serpentine filled with vapor and hence without further phase change possible, thus limiting the heat transfer and leading to saturation (dryout).

IV. Conclusions

This Paper have designed, tested and characterized an experimental setup for controlled localized nucleate boiling of regular trains of vapor bubbles injected in a capillary crossflow. A pyramidal cavity has been employed for practical reasons of construction, but the shape of the nucleation cavity can vary within certain conditions: it is assumed to have a planar side that will be in contact with the hot surface, at its section must keep its shape and increase its lateral dimension monotonously with distance to a vertex point. In this Paper's case this section was triangular, but it could be also semicircular (conical cavity) or otherwise. The device operation has been shown to be independent from gravity level, and constitutes the combination for the first time of (i) controlled nucleation at boiling sites, (ii) flow boiling, and (iii) slug flow conditions. By performing experiments both on ground and in microgravity (drop tower), this Paper has proved its performance as a method to tame the nucleation process (usually a very erratic, noisy and elusive phenomenon), and to produce vapor bubbles with a regular pace and size. These results show that the performance of this device is insensitive to gravity up to Bond numbers at least Bo $\sim$ 1. The resulting slug flow could then be transported by a pipe for other purposes of practical or fundamental interest.

Actual vapor nucleation was induced by a heated metallic surface near the tip of the cavity, and thanks to the opening geometry, bubbles are passively driven by surface tension towards the crossflow at the capillary where they are injected into. This Paper has carried out a comprehensive study of the performance of the nucleating device, by monitoring the frequency of bubble formation and the bubble volume, for different experimental parameters, namely pressure and metal temperature. In particular it has identified three operating modes of the device: Mode A, with a bubble train moving inside the cavity; Mode B, with a large vapor bubble detaching smaller ones which are periodically released; and Mode C, in which the cavity is completely filled of vapor and drag forces from the crossflow pinch-off small bubbles that are incorporated into the crossflow. In the three modes the device performs by generating very regular and periodic successions of vapor bubbles whose characteristics can be controlled. In particular the size dispersion is remarkably small compared to other boiling setups in microgravity. We have constructed a phase diagram separating the three operating modes in the parameter space.

For the Mode A this Paper has studied the dynamic of the bubbles inside the cavity, before the injection into the flow.

A different behavior of the bubbles was found, depending on whether they are in contact with the metallic surface or not. In particular, when in contact with the metallic part the velocity is roughly constant and the shape in invariant, so the bubble volume has a cubic dependence with the distance to the tip. However when the bubble is in contact with all insulating surfaces this dependence is approximately linear.

To illustrate the use of the device, a simple characterization of the transport of the vapor slug flow through a capillary has been performed, differentiating the gravity and the microgravity cases. During this transport the bubbles characteristics kept changing with time due to phase change. It can also be seen how the study of the evolution of bubbles along a pipe on a given thermal environment can be facilitated by the use of a controllable monodisperse and periodic slug flow.

Finally, this Paper has also illustrated possible uses of the device for considering the injection of the slug flow outcome into a heat exchanger for heat transfer applications. The injection of the pre-generated small vapor bubbles does permit the phase change, and the corresponding contribution to the heat transfer, for very low temperature differences without the need of nucleating the vapor inside the exchanger. Good control of the characteristics of the injected slug flow, and the fact that bubble nucleation is produced prior to the region of interest for heat exchange, provides a valuable freedom to optimize the performance of heat exchanger in a variety of conditions.

In some way this is a similar procedure to what proposed by Xu *et al.* [20], in which a microheater operating at a desired frequency generated seed bubbles, at the scale of 10 μm, which could stabilize flow at the microchannels where the boiling occurs. The main difference between both systems is that the current one does not require any active control of the generation frequency. Instead a robust and very regular generation of much larger vapor bubbles is passively achieved by the geometry of the cavity and controlling the heating conditions there, independently from the heat exchanger.

In all, the use of this nucleating device opens new possibilities for the study of transport and applications of biphase flows with phase change. The vapor bubbles are generated in a controlled and gravity-insensitive way, and can be orderly transported for subsequent study or practical applications. Specifically, new heat exchange correlations could be developed in optimized conditions. From a fundamental point of view, this method could be used to generate novel configurations of bubble suspensions in larger containers, to study the statistics of bubble coalescence, and in general the properties of turbulent bubble dispersions in microgravity, for instance injecting such vapor-liquid slug flows into controled turbulent flows, such as in [13].

Acknowledgments

References

[1] McQuillen, J., Rame, E., Kassemi, M., Singh, B., and Motil, B., "Results of the Workshop on Two-Phase Flow, Fluid Stability and Dynamics: Issues in Power, Propulsion, and Advanced Life Support Systems," NASA Glenn Research Center and National Center for Microgravity Research, NASA/TM—2003-212598, 2003.

[2] Di Marco, P., "Review of reduced gravity boiling heat transfer: European research," *Journal of the Japan Society of Microgravity Application*, Vol. 20, No. 4, 2003, pp. 252–263.

[3] Karayiannisa, T. G., and Mahmoud, M. M., "Flow boiling in microchannels: Fundamentals and applications," *Applied Thermal Engineering*, Vol. 115, 2017, pp. 1372–1397. URL https://doi.org/10.1016/j.applthermaleng.2016.08.063.

[4] Broussard, R. A., and Westwater, J. W., "Diameter and velocity effects for cross-flow boiling," *AIAA journal*, Vol. 23, No. 10, 1985, pp. 1615–1620. URL https://doi.org/10.2514/3.9132.

[5] Baldassari, C., and Marengo, M., "Flow boiling in microchannels and microgravity," *Progress in Energy and Combustion Science*, Vol. 39, No. 1, 2013, pp. 1–36. URL https://doi.org/10.1016/j.pecs.2012.10.001.

[6] Konishi, C., and Mudawar, I., "Review of flow boiling and critical heat flux in microgravity," *International Journal of Heat and Mass Transfer*, Vol. 80, 2015, pp. 469–493. URL https://doi.org/10.1016/j.ijheatmasstransfer.2014.09.017.

[7] Carrera, J., Ruiz, X., Ramírez-Piscina, L., Casademunt, J., and Dreyer, M., "Generation of a Monodisperse Microbubble Jet in Microgravity," *AIAA Journal*, Vol. 46, No. 8, 2008, pp. 2010 – 2019. URL https://doi.org/10.2514/1.33283.

[8] Arias, S., Ruiz, X., Casademunt, J., Ramírez-Piscina, L., and González-Cinca, R., "Experimental study of a microchannel bubble injector for microgravity applications," *Microgravity Science and Technology*, Vol. 21, No. 1-2, 2009, pp. 107–111. URL https://doi.org/10.1007/s12217-008-9060-1.

[9] Arias, S., González-Cinca, R., Ruiz, X., Ramírez-Piscina, L., and Casademunt, J., "Characterization of the performance of a minibubble generator in conditions relevant to microgravity," *Colloids and Surfaces A: Physicochemical and Engineering Aspects*, Vol. 365, No. 1, 2010, pp. 52–55.

[10] Arias, S., and Montlaur, A., "Numerical study and experimental comparison of two-phase flow generation in a T-junction," *AIAA Journal*, Vol. 55, No. 5, 2017, pp. 1565–1574. URL https://doi.org/10.2514/1.J055387.

[11] Bitlloch, P., Ruiz, X., Ramírez-Piscina, L., and Casademunt, J., "Spatial Structure and Velocity Fluctuations in Turbulent Bubble Jets in Microgravity," *International Journal of Transport Phenomena*, Vol. 12, No. 3-4, 2011, pp. 189–197.

[12] Bitlloch, P., Ruiz, X., Ramírez-Piscina, L., and Casademunt, J., "Turbulent Bubble Jets in Microgravity. Spatial Dispersion and Velocity Fluctuations," *Microgravity Science and Technology*, Vol. 27, No. 3, 2015, pp. 207–220. URL `https://doi.org/10.1007/s12217-015-9436-y`.

[13] Bitlloch, P., Ruiz, X., Ramirez de La Piscina, L., and Casademunt, J., "Generation and control of monodisperse bubble suspensions in microgravity," *Aerospace Science and Technology*, Vol. 77, 2018, pp. 344–352. URL `https://doi.org/10.1016/j.ast.2018.03.009`.

[14] Bitlloch, P., Ruiz, X., Ramirez de La Piscina, L., and Casademunt, J., "Bubble dynamics in turbulent duct flows: Lattice-Boltzmann simulations and drop tower experiments," *Microgravity Science and Technology*, Vol. 30, No. 4, 2018, pp. 525–534. URL `https://doi.org/10.1007/s12217-018-9634-5`.

[15] Balachandar, S., and Eaton, J. K., "Turbulent dispersed multiphase flow," *Annual Review of Fluid Mechanics*, Vol. 42, 2010, pp. 111–133. URL `https://doi.org/10.1146/annurev.fluid.010908.165243`.

[16] Sridhar, K. R., Chao, B. T., and Soo, S. L., "Pressure drop in fully developed, turbulent, liquid-vapor annular flows in zero gravity," *AIAA journal*, Vol. 30, No. 4, 1992, pp. 1016–1026. URL `https://doi.org/10.2514/3.11022`.

[17] Poniewski, M. E., and Thome, J. R., *Nucleate boiling on micro-structured surfaces*, Heat Transfer Research, Inc., Warsaw (Poland) and Lausanne (Switzerland), 2008.

[18] Xu, J., Gan, Y., Zhang, D., and Li, X., "Microscale boiling heat transfer in a micro-timescale at high heat fluxes," *Journal of Micromechanics and Microengineering*, Vol. 15, No. 2, 2004, p. 362. URL `https://doi.org/10.1088/0960-1317/15/2/017`.

[19] Xu, J., Shen, S., Gan, Y., Li, Y., Zhang, W., and Su, Q., "Transient flow pattern based microscale boiling heat transfer mechanisms," *Journal of Micromechanics and Microengineering*, Vol. 15, No. 6, 2005, p. 1344. URL `https://doi.org/10.1088/0960-1317/15/6/028`.

[20] Xu, J., Liu, G., Zhang, W., Li, Q., and Wang, B., "Seed bubbles stabilize flow and heat transfer in parallel microchannels," *International Journal of Multiphase Flow*, Vol. 35, No. 8, 2009, pp. 773–790. URL `https://doi.org/10.1016/j.ijmultiphaseflow.2009.03.008`.